Atmospheric Research 187 (2017) 1–15

Contents lists available at ScienceDirect

Atmospheric Research

journal homepage: www.elsevier.com/locate/atmosres

Observational and modeling study of a mesoscale convective system during the HyMeX — SOP1

S Dafis [a,b,*], K Lagouvardos [b], V Kotroni [b], T M Giannaros [b], A Bartzokas [a]

[a] Laboratory of Meteorology, Department of Physics, University of Ioannina, 45110 Ioannina, Greece
[b] National Observatory of Athens, Institute for Environmental Research and Sustainable Development, Vas. Pavlou & I. Metaxa, 15236 Athens, Greece

ARTICLE INFO

Article history:
Received 16 June 2016
Received in revised form 16 November 2016
Accepted 2 December 2016
Available online 22 December 2016

Keywords:
Lightning
WRF
Sensitivity
Microphysics
Convective parameterization schemes
HyMeX

ABSTRACT

An intense and fast moving convective line that crossed Massif Central/Cévennes-Vivarais area (south France) during the field campaign of Hydrological Cycle in Mediterranean Experiment (HyMeX) — Special Observing Period 1 (SOP1) is examined. The mesoscale analysis demonstrates a complex convective system with a V-shape in the Infrared (IR) satellite imagery and a squall line pattern on the radar imagery. Ground stations observed up to 60 mm h^{-1} of rain accumulation, while the lightning activity, as observed by 4 detection networks, was also exceptionally high. The Weather Research and Forecasting (WRF) model was used to simulate this convective episode and sensitivity tests were performed with various microphysics and convective parameterization schemes. Satellite data from Meteosat SEVIRI Rapid Scanning Service were used in conjunction with radar, lightning and rain gauge data to conclude on the best simulation for which WRF model exhibits a rather precise and realistic distribution and evolution of the precipitation patterns. Finally, a study of the microphysics was performed indicating the interconnection of graupel with lightning activity, confirming recent results, compared against a sophisticated hydrometeor classification radar algorithm and lightning data.

1. Introduction

Precipitation is probably the most important weather parameter to the public and thus the most important part of any weather forecast, albeit among the most difficult to forecast. Due to the nature of precipitation, its spatial and temporal distribution is highly variable and intermittent on small scales, thus constituting one of the most chaotic of all atmospheric variables (Fritsch et al., 1998).

Precipitation is also a potentially major hazard, with flash flooding being a regular feature on the news. In the Mediterranean area heavy precipitation often produces floods and it is one of the most common severe weather types that, when accompanied with local vulnerability, it turns into socio-economic high impact weather. Several efforts have been devoted into building up flood databases for the Mediterranean with the most recent one being that produced by Llasat et al. (2013), complemented by Papagiannaki et al. (2013) in the frame of the international, 10-yr concerted Hydrological Cycle in Mediterranean Experiment (HyMeX) program (http://www.hymex.org/) (Drobinski et al., 2014).

In the European Severe Weather Database (ESWD) (Dotzek et al., 2009) there are >2000 reports of heavy rainfall events in France during the period 1970–2015, with half of them (1055) referring to the Massif Central/Cévennes-Vivarais region (South France). Southern France is a region prone to devastating flash flood events, particularly during autumn. In the past decades, devastating flash floods responsible for human casualties, and heavy damage or destruction of housing and infrastructures have occurred in the area, including the events of Vaison-la-Romaine (Senesi et al., 1996), Aude (Ducrocq et al., 2003) and Gard (Ducrocq et al., 2004; Delrieu et al., 2005) on 22 September 1992, 12–13 November 1999 and 8–9 September 2002, respectively. The total economic damages were estimated at €1.2 billion for the Gard 2002 flash flood event (Huet et al., 2003) and €3.3 billion for the Aude 1999 flash flood (Lefrou et al., 2000). The mesoscale triggering and sustaining ingredients of three torrential rain events over southern France were examined by Nuissier et al. (2008) by using the Meso-NH non-hydrostatic mesoscale numerical model, which reproduced fairly well the low-level mesoscale environments associated with the three high-precipitation events. In addition, Ducrocq et al. (2008) performed high resolution numerical experiments and sensitivity tests of three heavy precipitation events with the Meso-NH model in Cévennes, Aude and Gard areas and focused on the orographic forcing of the Massif Central relief, by evaluating the general role of the mountain range on the intensification of low level convergence. Furthermore, Godart et al. (2010) tried to identify the climatology associated with deep convective and shallow banded convection in the Cévennes-Vivarais area by using the Meso-NH model. Lagouvardos et al. (2013) performed high-resolution simulations of a convective event in Cévennes-Vivarais area by using

* Correspondence author.
E-mail address: sdafis@noa.gr (S. Dafis).

http://dx.doi.org/10.1016/j.atmosres.2016.12.001
0169-8095/

the MM5 model and explored the impact of assimilating lightning observations on the improvement of rainfall forecast with promising results.

Heavy precipitation in the Mediterranean has been found to be associated with intense cyclones or the result of deep moist convection, in particular that produced by mesoscale convective systems (MCS) (Jansa et al., 2014; Flaounas et al., 2015, 2016). Large amounts of precipitation can accumulate in less than a day when a MCS stays over the same area for several hours (Parker and Johnson, 2000; Houze, 2004). MCSs can be organized in linear systems and even if they are often characterized by less accumulated precipitation compared to stationary MCS due to their speed (Markowski and Richardson, 2010), they often produce severe wind gusts, tornadoes, hail and damaging lightning (Markowski and Richardson, 2010; Newman and Heinselman, 2012). Heavy precipitating events (HPEs) in southern France are often characterized by quasi-stationary behavior (Ricard et al., 2012) that results in significant precipitation amounts (typically >200 mm and, in extremely rare events, >500 mm in <24 or 48 h).

As the study of microphysical species and lightning activity of a convective storm is concerned, charging within convective clouds occurs in a region referred to as the "charging zone", with a limited vertical extent, and involves collisions between graupel and ice crystals in the presence of supercooled liquid water. The upper limit of the charging zone is the level above which these three types of hydrometeor do not coexist which typically lies between the −15 °C and −30 °C isotherms. Lund et al. (2009) identified graupel as the microphysical species having the highest probability of being associated with lightning initiation and also noticed that upper-level lightning initiation (within a normal tripolar charge structure) did arise at the interface between ice and graupel, whereas only graupel seemed to occur for low-level lightning initiation occurrences. Modeling and observational studies also suggest a high correlation between total lightning rate and flux product components, such as graupel volume and the updraft volume (Wiens et al., 2005), thus if a model tends to simulate correctly the lightning distribution, it is important to simulate the vertical distribution of microphysical species, as well as the kinematics within convective clouds.

The aim of the present study is to analyze a strong linear MCS observed on 24 September 2012, during the Intensive Observation Period 6 (IOP6) of the HyMeX Special Observing Period 1 (SOP1) (Drobinski et al., 2014; Ducrocq et al., 2014). The main objective of the HyMeX — SOP1 field campaign (September–November 2012) was to collect an extensive dataset of measurements to better understand the physical processes that lead in severe weather events in northwest Mediterranean basin. In order to achieve that, numerous instruments were deployed in South France and NW Italy during the fall 2012, such as rain gauges, GPS sensors, mobile radars, lightning detectors (e.g. HyLMA) as well as shipborne and airborne means. Observations over the sea were collected with a combination of platforms navigating, drifting and fixed. Moreover, operational networks were used, like ARAMIS - Météo-France radar network and lightning detection systems (more information are provided in Section 2).

During the IOP6 event accumulated rainfall exceeded 60 mm in 1 h and exceptional lightning activity was recorded (Defer et al., 2015; Ribaud et al., 2016). Hally et al. (2014) studied the sensitivity of simulated rainfall fields to physical and initial and boundary condition uncertainties of the IOP6 event using an ensemble approach. The authors used analyses from the AROME, AROME-WMED, ARPEGE and ECMWF operational models as initial and boundary conditions for the research model Meso-NH at a fine horizontal grid spacing of 2.5 km and they found a low level of agreement with the observations of accumulated precipitation. In a second step, they used the most accurate member of this ensemble as a control simulation and three further ensembles were constructed in order to study uncertainties related to cloud physics and surface turbulence parameterizations.

In addition to the study of the IOP6 event, the objectives of the current work are: (a) to investigate the sensitivity of quantitative precipitation forecasts to different microphysical and cumulus parameterization schemes implemented in WRF model; (b) to explore the role of the increase of grid spacing in the improvement of the quantitative precipitation forecast and; (c) to study the model microphysical characteristics of the MCS in relation with the lightning activity.

The study is organized as follows: In section 2 we describe the synoptic and mesoscale conditions that triggered this convective episode, in section 3 we introduce the model configuration with the 9 simulations we performed for the sensitivity tests and we present the results of our verification method. Finally, section 4 is devoted to conclusions and prospects.

2. Observational analysis of the MCS

2.1. Synoptic setup

On 24 September 2012, the period of heavy precipitation over Cévennes-Vivarais (CV) region started just before midnight (00:00 UTC) and lasted about 9 h. During the previous night, a predominant cyclonic vortex over Northern Europe shifted eastwards, stepping aside for another cyclonic vortex, which approached from the North Atlantic. A strengthening depression from the Bay of Biscay incorporated into the circulation of the second vortex and the net result was a major cyclonic vortex, centered over United Kingdom (UK), which became the steering mechanism for the weather pattern in Western Europe (Fig. 1a). Over the West Mediterranean Sea, geopotential heights started to decrease with the formation of a weak ridge over the East Mediterranean. An approaching frontal discontinuity from the Northwest was marked by enhanced baroclinicity with the evolution of a distinct tropopause fold over the Ireland and the UK, bending into the system (Fig. 1d). This increase of baroclinicity resulted in a rapid deepening phase, which started around the beginning of the period of interest (00:00 UTC on September 24). Moreover, CV was under the left exit of a mid-level jet streak (Fig. 1b) while a 500 hPa vorticity lobe crossed the area from west to east and moved into this unstable and strongly sheared air mass in South France (Fig. 1c).

2.2. Analysis of surface and radiosonde data

For the observational analysis, surface and radiosonde observations collected during SOP1 were used. These data include both observations by rain gauges especially installed for the SOP1 as well as observations from the operational Météo-France network. According to radio sounding measurements in Nimes-Courbessac (00:00 UTC 24 September - Fig. 2), steep lapse rates in mid-troposphere (8 K km^{-1}) and abundant influx of moist Mediterranean air from the south result in roughly 1200 J kg^{-1} of mixed layer convective available potential energy (MLCAPE), which overlaps with deep layer shear 0–6 km (DLS) values of 25 m s^{-1} (Fig. 2b). Similar shear magnitude is also found in the lower troposphere (15–20 m s^{-1} of 0–3 km bulk shear). Not only the speed shear, but also storm relative environmental helicity (SREH) is enhanced with values in excess of 300 m^2 s^{-2} in the lowest 3 km ahead and along the cold front. Precipitable water (PWTA) is calculated to 34 mm and the convective inhibition (CIN) near 750 hPa was not enough to suppress convection.

Fig. 3 shows the spatial distribution of the 1679 rain gauges, as well as the amount of accumulated precipitation in 12 h period, between 00:00 and 12:00 UTC, on 24 September 2012 inside the SOP1 domain along with the three subdomains of Cévennes-Vivarais (CV) and Corsica (CO) in France and Liguria-Tuscany (LT) in Italy as adopted by HyMeX (Ducrocq et al., 2014). The maximum rain accumulation was 100 mm in 12 h, 91.3 mm during 00:00–06:00 UTC, and 68.7 mm during the period 06:00–12:00 UTC. It is also worth mentioning that 16 rain gauges exceeded 60 mm in 12 h, while 189 stations exceeded 20 mm of rain. The most intense precipitation was recorded in the southeastern flank of Massif Central mountain range, at Gard and Vaucluse departments,

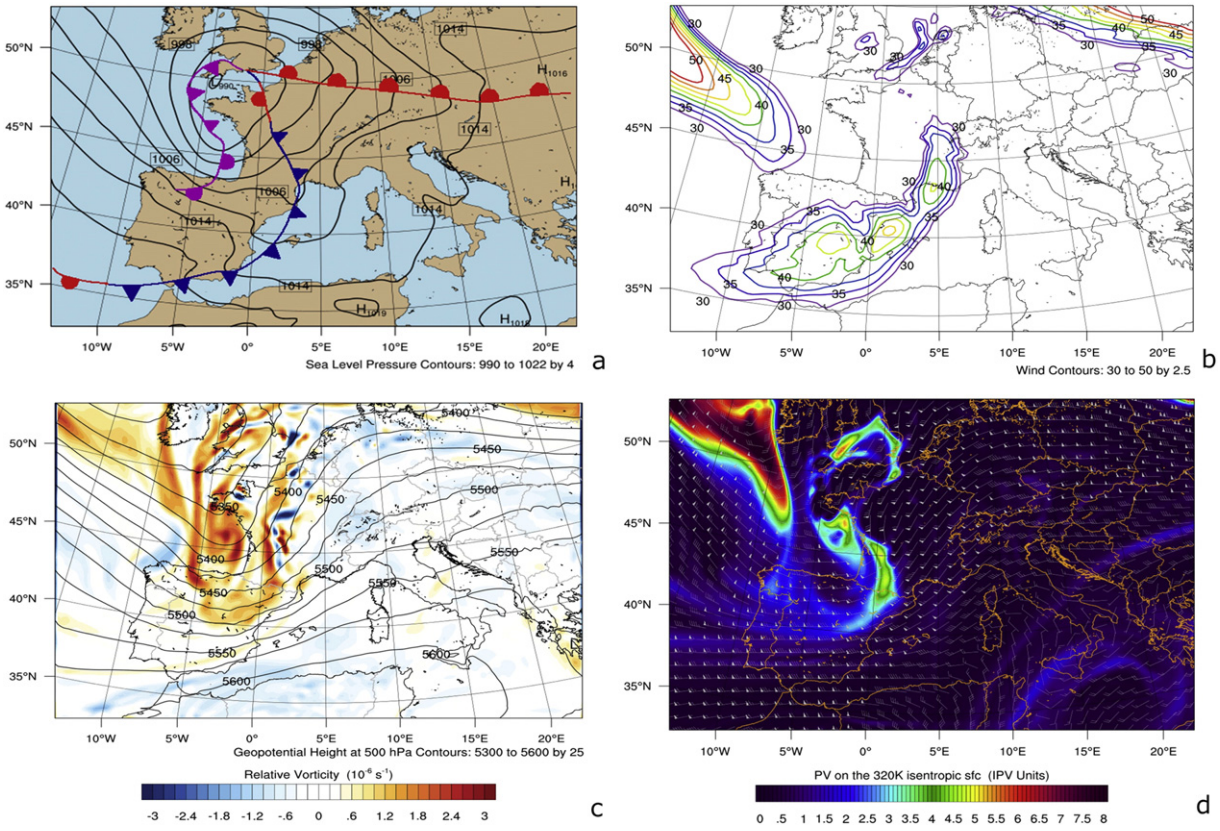

Fig. 1. ECMWF analysis at 00:00 UTC 24 September 2012: (a) Sea-level pressure, (b) wind speed at 300 hPa (only values exceeding 30 m s^{-1} are shown), (c) relative vorticity and geopotential height at 500 hPa, (d) potential vorticity on the 320 K isentropic surface in PV units (1 PVU = 10^{-6} m^{-2} s^{-1} K kg^{-1}).

between 02:00 and 03:00 UTC, when Mejannes-le-Clap station reached 60 mm in 1 h (max 76.6 mm in 4 h), and the rain gauge at Salindres accumulated 16 mm in <6 min (max 77.1 mm in 3 h). There are also nine stations that exceeded 40 mm in the Ardèche and Drôme departments as well as one station in Alpes-Maritimes department, where a stationary MCS was formed in the morning hours of 24 September 2012.

2.3. Analysis of satellite and radar imagery

The retrieval of satellite images from the EUMETSAT SEVIRI Rapid Scanning Service (RSS) and ground radar from Nimes (Météo-France ARAMIS network) show the precise position of the MCS with a V-shape feature visible in the infrared channels (e.g. Water Vapor channel

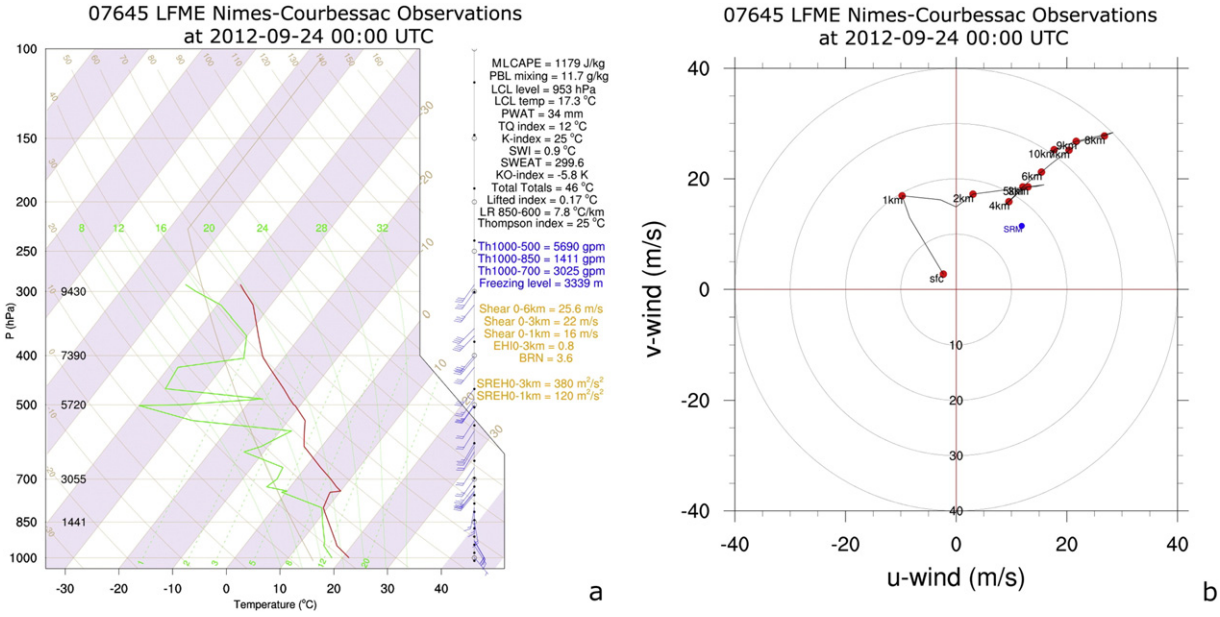

Fig. 2. (a) Radiosonde measurements from Nimes-Courbessac station and (b) the derived hodograph, with each red dot representing the wind speed and the blue dot representing the storm motion (SRM) in m s^{-1} at 00:00 UTC on 24 September 2012.

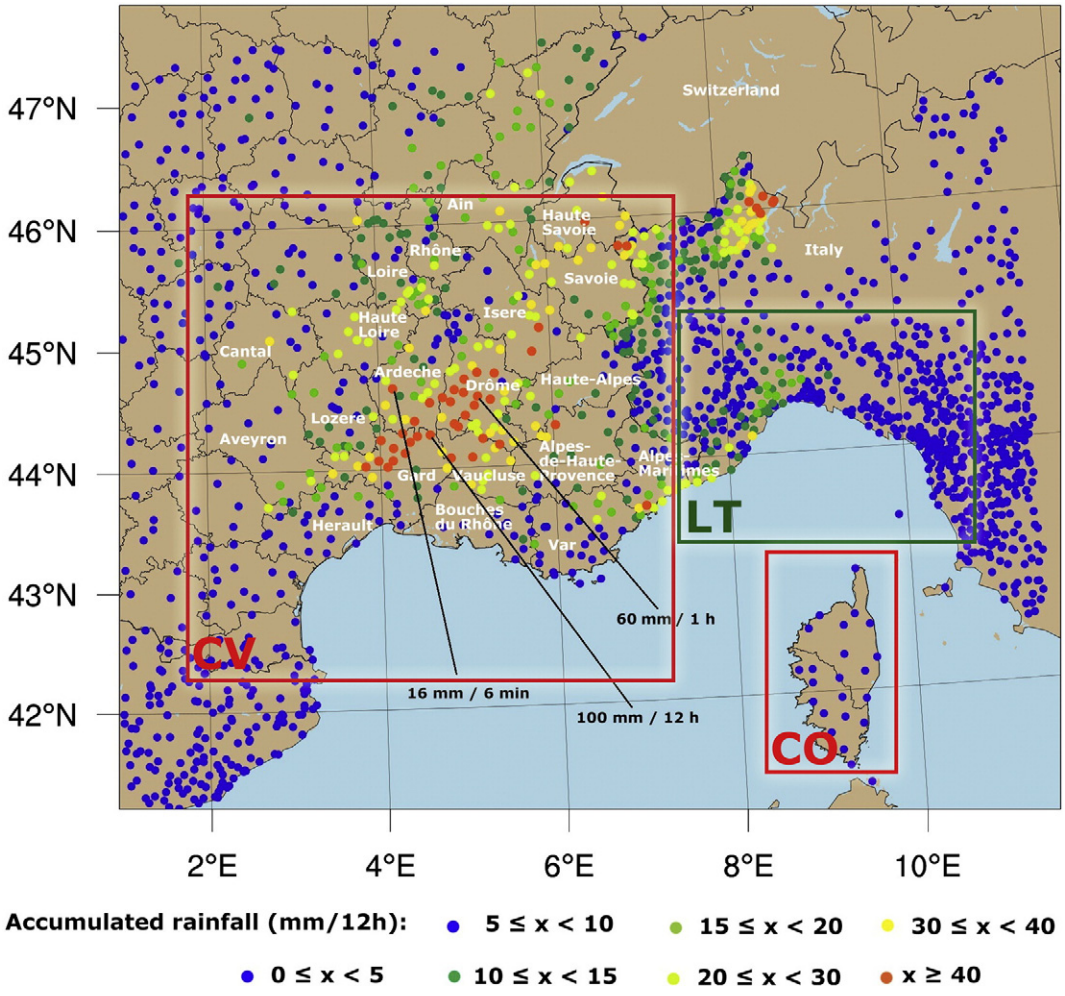

Fig. 3. Spatial distribution of the 1679 rain gauges with the 12-hour accumulated precipitation (mm 12 h^{-1}) ending at 12.00 UTC, 24 September 2012 inside the SOP1 domain along with the three subdomains of Cévennes-Vivarais (CV) and Corsica (CO) in France and Liguria-Tuscany (LT) in Italy as adopted by HyMeX (Ducrocq et al., 2014).

- WV6.2 μm) and a linear convective signature on the radar echoes at 03:00 UTC (Fig. 4a–b). In Fig. 4a, it is clearly visible a "dark area" that indicates a northeastward dry intrusion in the mid-levels, from lower stratosphere or upper troposphere, which overruns the lower-lever warm, moist and rainy region. This dry intrusion is also evident in the Nimes-Courbessac sounding in Fig. 2. Dry intrusions like this, convey cold, dry high potential vorticity (PV) air masses and play an important role in enhancement of convective phenomena (Lagouvardos and

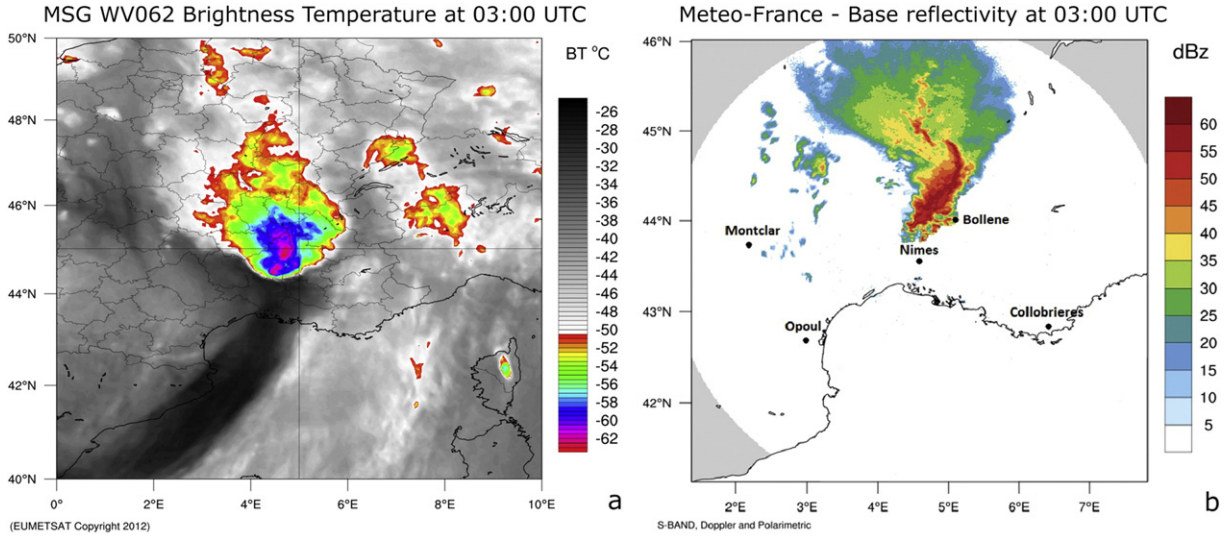

Fig. 4. (a) Brightness temperature from SEVIRI RSS derived by the 6.2 μm channel at 03:00 UTC and (b) base reflectivity from operational S-band radar in Nimes at 03:00 UTC and the location of the S and C-band radars of ARAMIS network (Météo-France).

Kotroni, 2000; Shuai et al., 2009). In addition, previous studies have shown that while the dry intrusion descends, approaching the lower-level moist air, with high equivalent potential temperature that is moving upwards, instability over this region is enhanced (Browning and Golding, 1995; Gao and Cao, 2007). The analysis of Nimes radar imagery (Fig. 4b) also shows characteristics of a bow echo system while approaching Nimes and Montclar radar sites (Bousquet et al., 2015). Usually, linear convective systems are triggered by a cold front or a convergence line, while in the current analysis both conditions are met. Vertical cross sections of radial wind velocity (not shown) depict two distinct relative flows, one that is entering the system from ahead and rises fast to the back of the storm cells and another mid-level jet that enters the system from behind and descends to the surface (Ribaud et al., 2016). Ground stations reported wind gusts up to 100 km h^{-1} during the period from 02:00 to 03:00 UTC, on 24 September. In the horizontal radar cross section shown in Fig. 4b, it is noticeable a leading line of convection with heavy rain (CV region) moving fast east-southeastward which is followed by an area of stratiform precipitation zone in the northern parts of Ardèche and Drôme administrative departments.

2.4. Analysis of lightning data

Three lightning detection systems were used in conjunction with satellite and radar data to better investigate the life cycle of this convective episode. For this case study, we used the Arrival Time Difference network - ATDnet (Bennett et al., 2010), the EUropean Cooperation for LIghtning Detection - EUCLID (Poelman et al., 2012) and the ZEUS (Kotroni and Lagouvardos, 2008; Lagouvardos et al., 2009). All of the aforementioned systems are able to detect cloud to ground (CG), while EUCLID can partly detect intra-cloud (IC) strokes. For the analysis, strokes and not flashes are considered, as the criteria for space and time separation used to group strokes to flashes differ in the literature (e.g. Cecil et al., 2014 ; Anderson and Klugmann, 2014). Indeed, Yair et al. (2014) presented a very interesting analysis and showed how the selection of these criteria affects the calculated multiplicity. Fig. 5 shows the lightning strikes over southern France and northwest Italy as they were detected by the three networks during the period from 00:00 to 12:00 UTC, on 24 September 2012. The graph in Fig. 5d summarizes the total number of the strokes from 00:00 to 09:00 UTC (i.e. the time period when the storm was inside the SOP1-CV sub-domain) accumulated at 1-hour intervals.

Overall, the lightning activity can be divided into four distinct periods: The first period (LP1) from 00:00 to 02:00 UTC, which was characterized by intense lightning activity with 5270 lightning strikes recorded by the EUCLID network. During LP1, the maximum 5-min composite reflectivity values were fluctuating from 46 to 63 dBz and the coldest BT measured by the infrared channel 10.8 μm of SEVIRI was −63 °C collocated with the maximum reflectivity values (not shown). The second period (LP2) started at 02:00 UTC, lasted for 2 h

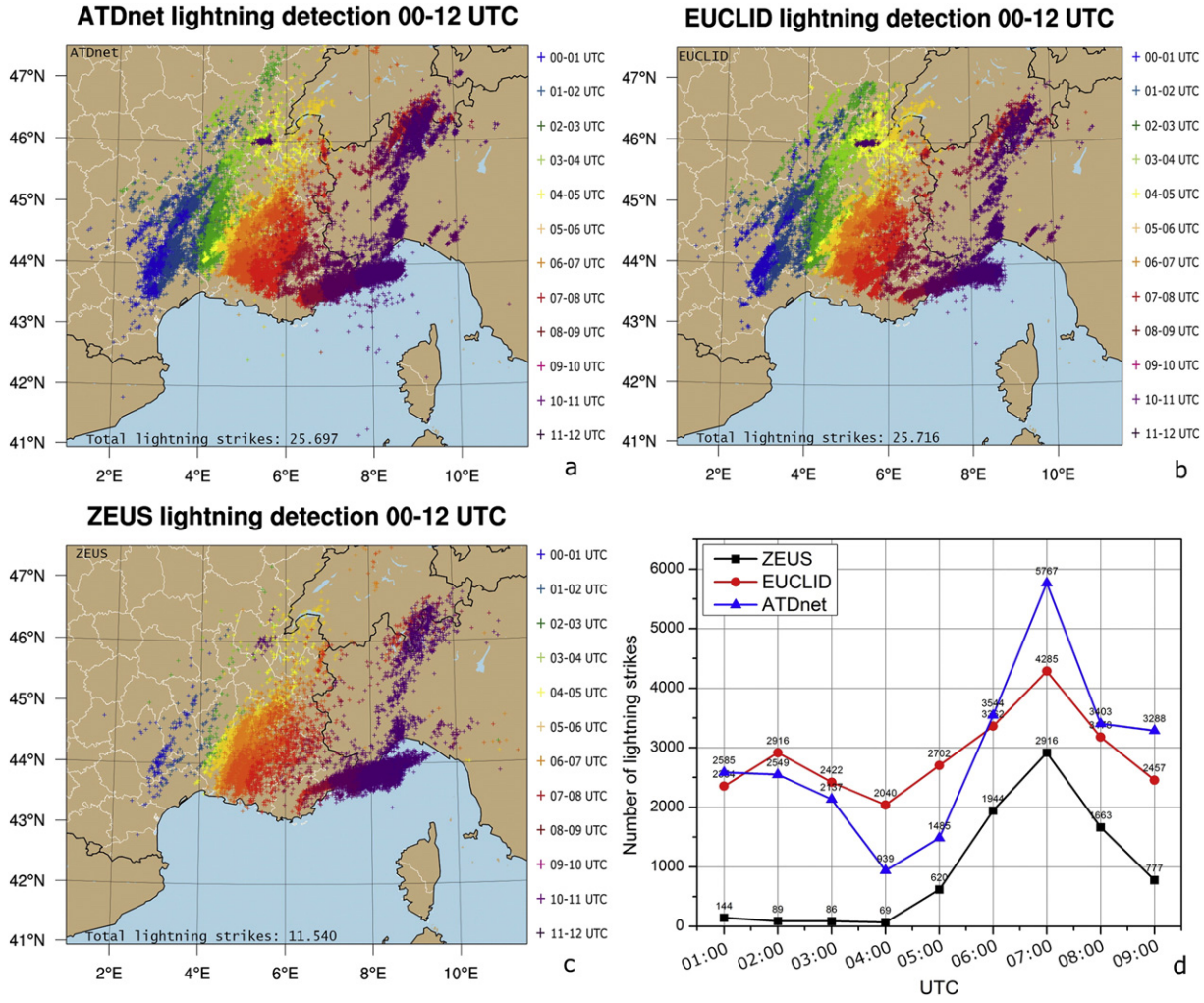

Fig. 5. Lightning activity as recorded by (a) ATDnet (CG), (b) EUCLID (CG/IC), and (c) ZEUS (CG) networks between 00:00 and 12:00 UTC on 24 September 2012 with colors representing the time intervals. (d) Plot showing the number of lightning strikes recorded by each network inside the SOP1 domain from 00:00 until 09:00 UTC.

and was associated with a gradual decrease of the lightning activity, very cold cloud top heights, as the minimum BT was −64 °C at 03:00 UTC and a sharp decrease of reflectivity values between 03:00 and 03:55 UTC. The duration of the third period (LP3) was the longest, from 04:00 to 07:00 UTC and it was characterized by a lightning peak activity with a total of 10,796 lightning strikes recorded by the ATDnet network. The maximum lightning activity was recorded between 06:00 and 07:00 UTC. Based on the EUCLID system during the maximum of the lightning activity 68% of the strokes were IC but also CG strokes were progressively increasing the whole period LP3. In the fourth period (LP4; 07:00–09:00 UTC), there was again a gradual decrease of the lightning activity associated with the dissipation of the MCS by a visual inspection on the satellite and radar imagery.

At 05:00 UTC, in the satellite imagery, an overshooting top with cloud top height of −60 °C is evident, associated with the most intense CG lightning activity (1324 strikes in 30 min) occurring at the rapid developing storm cell, a few kilometers southwest of the dissipating cluster (Fig. 6a). In Fig. 6b, the EUCLID CG strokes are plotted over the satellite imagery for the period 04:45–05:15 UTC and they are almost collocated with the depression of brightness temperatures, while most of the anvil area is not responsible for the initiation of CG strokes. Radar derived reflectivity composite from Nimes' site recorded areas of 52–56 dBz, collocated with the coldest cloud top heights (not shown). Furthermore, the dry slot has moved eastward compared to satellite imagery at 03:00 UTC (Fig. 4a), over passing the MCS which has stalled NE from Nimes, and by 07:00 UTC it is found over Italy.

3. Numerical modeling

3.1. Model setup

In order to perform the simulations of this convective episode, the Weather Research and Forecasting (WRF) non-hydrostatic model (Skamarock et al., 2008) was used with three nested grids that allowed us to evaluate the model's forecasting skill in reproducing the large-scale forcing ingredients in a coarse domain (d01) of 18 km horizontal grid size (185 × 130 grid points) and the accumulated rainfall in two higher resolution domains (d02 and d03) of 6 and 2 km horizontal grid increment (256 × 196 and 436 × 346 grid points, respectively). The coarse domain covers the major part of Europe while the second one covers France and parts of Northwest Mediterranean Sea. The area of the finest domain focuses on the HyMeX — SOP1 area in the CV region (Fig. 7). On the vertical axis, there are 40 unevenly spaced full sigma levels.

Several physical parameterization schemes are available in the model for the boundary layer turbulence, the radiative transfer, the microphysics, and the cumulus convection. Concerning the choice of planetary boundary layer scheme (PBL), Yonsei University Scheme (YSU) was used which can accurately simulate deep vertical mixing in buoyancy-driven PBLs with shallow mixing in strong wind regimes (Hong et al., 2006). For radiative transfer, the schemes of Dudhia (1989) and RRTM (Mlawer et al., 1997) were used for shortwave and longwave radiation, respectively. The Unified Noah Land Surface model scheme (Tewari et al., 2004) was used as it performs well in capturing the surface heterogeneity and thus, surface emissivity.

The model was initialized using European Centre for Medium-Range Weather Forecasts (ECMWF) model analysis data at 0.25° × 0.25° horizontal grid increment, while the lateral boundary conditions of the coarse domain were updated every 6 h. The simulations started at 12:00 UTC 23 September 2012 and lasted for 36 h.

Using the aforementioned setup, a series of sensitivity tests were performed in order to explore the combination of microphysical (MP hereafter) and cumulus parameterization schemes (CPS) that better reproduces precipitation for the case study. The following MP schemes were tested: Thompson (NTH) (Thompson et al., 2008), Morrison (MOR) (Morrison et al., 2009) and Milbrandt and Yau (MIL) (Milbrandt and Yau, 2005) combined with the CPS: Grell and Freitas (GRF) (Arakawa, 2004), Kain-Fritsch (KF) (Kain, 2004) and Multi-scale Kain-Fritsch (MKF) (Zheng et al., 2015). The CPS was only activated in d01 and d02. Regarding MIL and MOR schemes, they are double moment microphysical schemes, with MIL resolving 7 microphysical species (cloud water, rain, ice, graupel, snow, supercooled water and hail) and MOR 6 species (not hail). Also NTH scheme cannot explicitly resolve hail, and can provide concentration information only for ice and rain. Moreover, as far as CPS schemes are concerned, KF is the most used mass flux cumulus scheme in mesoscale modeling and MKF is a modified version of KF with a new triggering function for high resolution grids. In addition, MKF compared to KF has a more efficient adjustment timescale for restoring the stability of the atmosphere, plus a new entrainment function and one of the reasons leading us to test it was that there were no case studies in Europe using it by the time our study was carried out. GRF has replaced the Grell-Devenyi scheme as it provides a smooth transition to cloud resolving scales (like MKF is supposed to) and it is a mass flux CPS, but the main difference with KF and MKF is that it provides parameterized downdrafts.

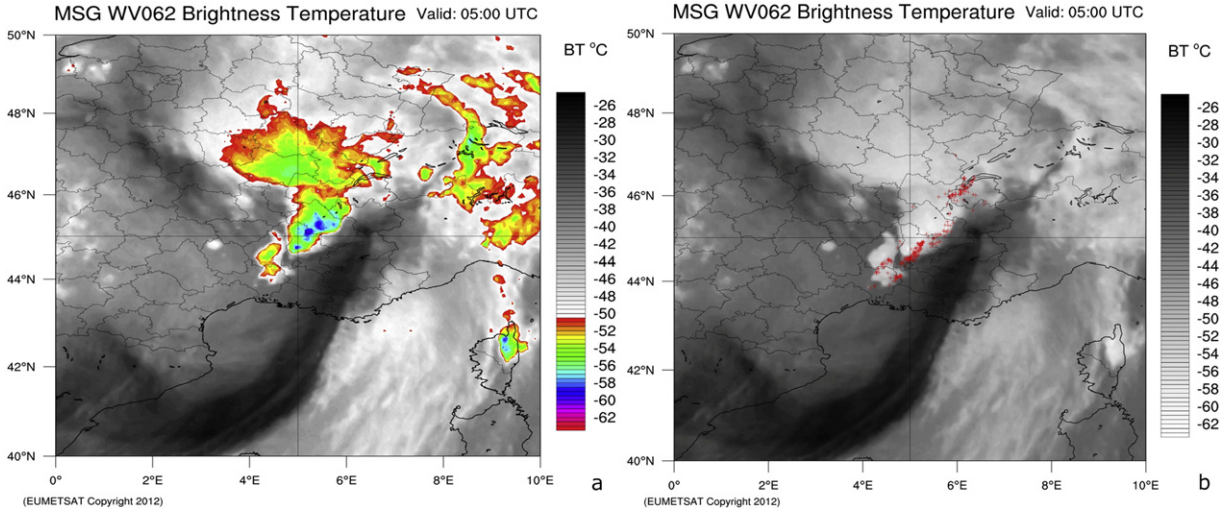

Fig. 6. (a) Brightness temperature (BT) of MSG WV 6.2 μm channel at 05:00 UTC and (b) EUCLID CG lightning strikes overlapped with BT at 05:00 UTC.

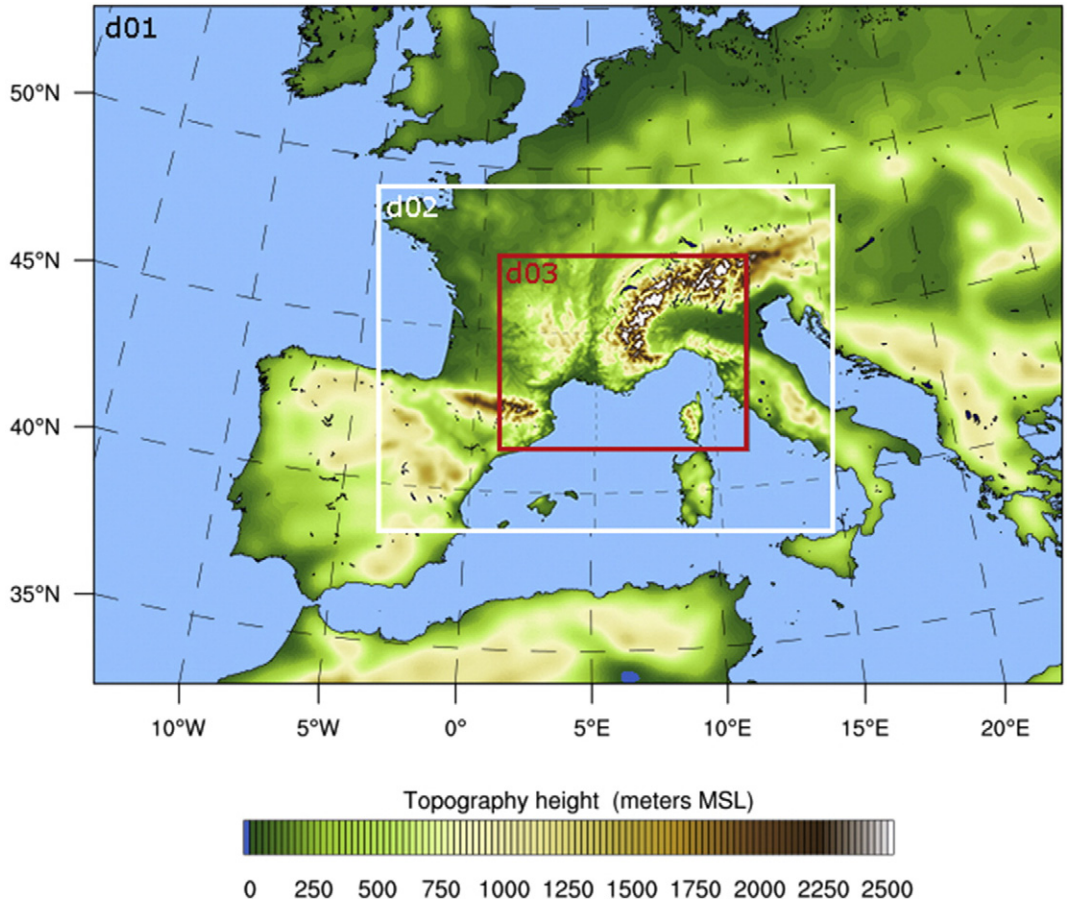

Fig. 7. The WRF coarse (d01) and the nested domains (d02, d03) with their topography.

3.2. Verification methodology

For the evaluation of model performance, precipitation data from 1679 rain gauges spread across the study area were used (Fig. 2). For the verification, a "best nearest neighbor" approach was adopted, examining the nine model grid points surrounding each rain gauge location and selecting the one showing the closest value to the observation. This approach was preferred in order to avoid penalizing model due to displacing predicted precipitation compared to the observed. The verification of precipitation was performed for 3 periods, from 00:00 UTC to 06:00 UTC (6 h), from 06:00 to 12:00 UTC (6 h) and from 00:00 to 12:00 UTC (12 h) on 24 September 2012. During the first period the MCS was totally inside the HyMeX — SOP1-CV domain, while during the second period and more specifically at about 09:00 UTC the system left the SOP1-CV domain. The verification procedure was carried out on a dichotomous decision basis, using paired modeled and observed precipitation values, and 2×2 contingency tables were constructed using 5 precipitation thresholds, namely above 1, 2.5, 5, 10 and 20 mm (Kotroni and Lagouvardos, 2001; Lagouvardos et al., 2003; Federico et al., 2004; Mazarakis et al., 2009), in order to compute three qualitative statistical parameters: probability of detection (POD), false alarm ratio (FAR) and Heidke skill score (HSS). Further, quantitative performance metrics were computed, including: frequency bias (BIAS), mean absolute error (MAE), standard deviation of forecast (σ_f), standard deviation of observations (σ_o), root mean squared error (RMSE) and correlation coefficient. For quantitative measures, the defined thresholds were: 0.1–2.5, 2.5–5, 5–10, 10–20, and >20 mm.

3.3. Verification results

Fig. 8a–b shows the POD results for the period 00:00–06:00 UTC, which depicts the ability of the simulations to correctly forecast the observed precipitation events. The unity is the perfect score, while zero is the lowest possible value. For d02 the configurations that use the MOR microphysical scheme seem to have the best skill in comparison to MIL and NTH for thresholds below 10 mm. Concerning the CPS, KF seems to have the best forecast skill. In the highest resolution domain (Fig. 8b), we have a significant improvement of POD for the higher thresholds, for the simulations MKF_MOR and MKF_NTH, with the MKF_MOR simulation having the best scores at all thresholds. For the period 06:00–12:00 UTC, POD scores in both domains are lower for the 20 mm threshold, but again we can notice better scores in the highest resolution domain than in d02 (not shown). As far as the longest verification period is concerned (00:00–12:00 UTC) we do not notice a significant change of the scores for thresholds below 5 mm, but slightly lower scores for the 10 mm threshold in the d03, except from those simulations that use the MKF CPS. For the 20 mm threshold, KF_MOR simulation is the best in d02 and MKF_MIL in d03 (not shown).

Furthermore, FAR scores for the first verification period are shown in Fig. 8c–d, with zero being the best score and unity the worst. Simulations have better FAR scores for thresholds above 2.5 mm, compared against the first verification period in d02 (Fig. 8c), with slightly better overall scores in d03 (Fig. 8d). During 06:00–12:00 UTC, FAR scores of all simulations are worse for thresholds 10 and 20 mm with the best scores found for the simulations that use the GRF scheme. For the 12-

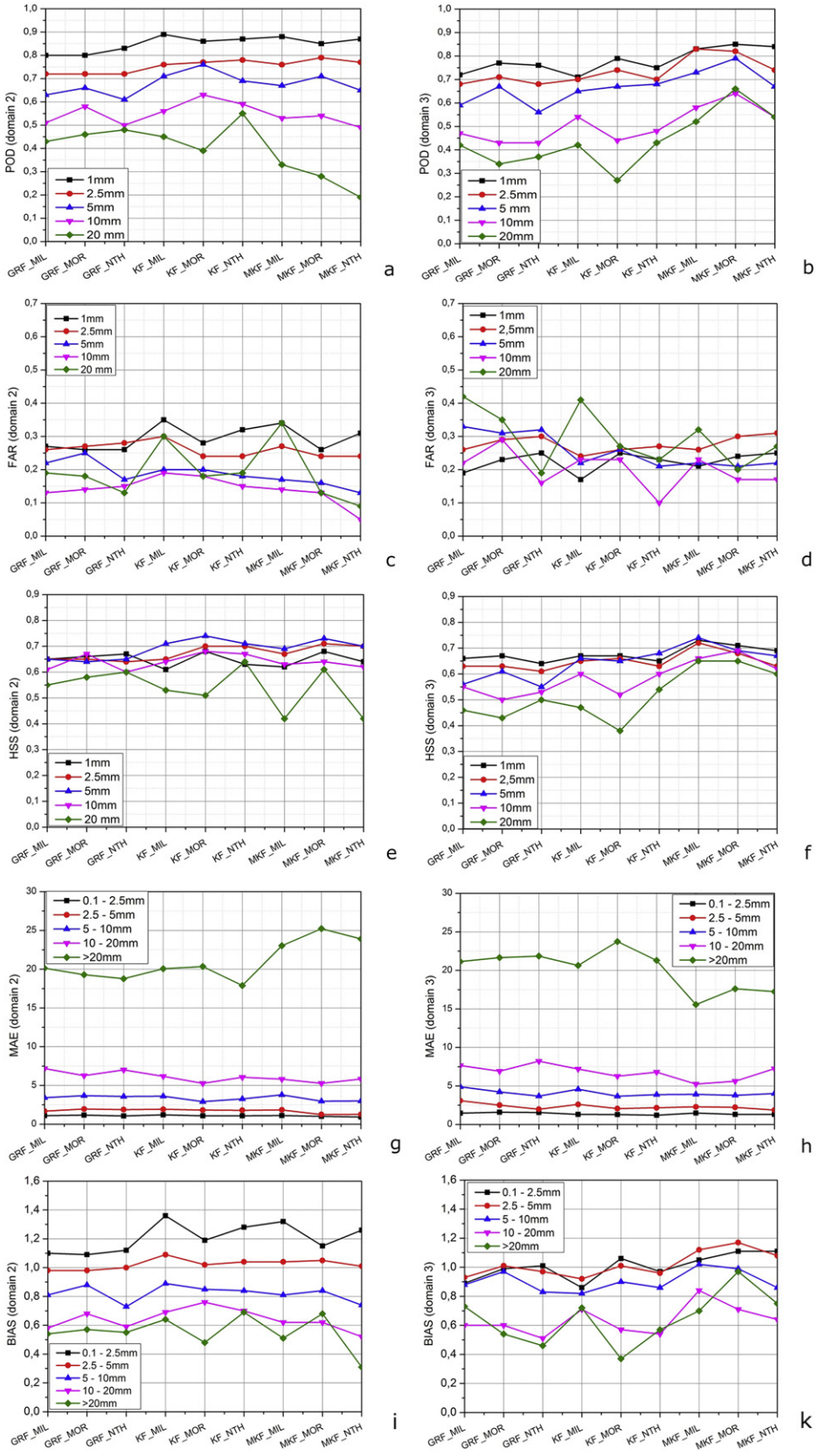

Fig. 8. (a–b) POD, (c–d) FAR, (e–f) HSS, (g–h) MAE and (i–k) BIAS for the 6-hour (00:00–06:00 UTC) precipitation forecasts for d02 and d03.

hour period of verification, in d02, simulations with GRF have also the best scores and in d03 KF_NTH and MKF_MOR have the best FAR scores for the highest threshold (not shown).

The Heidke Skill Score (HSS) is based on the hit rate and measures the fraction of correct forecasts (reference forecast) after eliminating the forecasts which would be correct due to random chance. Perfect

forecasts receive a Heidke score of one, equivalent to the reference forecasts receive a zero and forecasts worse than the reference ones, receive negative scores. Fig. 8e–f shows an increase of the HSS scores from d02 to d03 for MKF simulations, for the 20 mm threshold, even though MKF_MOR score is comparable to the lowest threshold scores in both domains. During 06:00–12:00 UTC we do not see a significant change of the HSS scores between the two domains, and again MKF_MOR has the highest score for the highest threshold. Also the KF simulations have higher scores than the GRF ones. For the 12-hour verification period, we have lower scores in d03 for MKF_MIL and MKF_MOR simulations compared to d02 for thresholds above 5 mm (not shown).

Investigation of the quantitative bias of forecast precipitation is performed through the inspection of mean absolute error (MAE) for which a perfect forecast equals zero and frequency bias (BIAS) with a perfect score equal to 1. For the first 6-hour verification period (Fig. 8g and h) we have an average MAE score of 20.6 mm and 20.2 mm for the range >20 mm in d02 and d03, respectively and as far as BIAS is concerned, we notice that the simulations using the MKF scheme are less biased in d03 than in coarser d02 (Fig. 8i and k). Moreover, for the lowest threshold and for the range 5–10 mm we have better scores in d03. MAE scores are much lower (~11 mm) during the period 06:00–12:00 UTC (not shown) for both domains and BIAS has values from 0.4 to 0.6 for simulations which use the GRF scheme for the range >20 mm (not shown), while again MKF scheme performs better than the rest (values from 0.8 to 1.2). Slightly lower MAE and BIAS scores are found for the 12-hour verification period, for the ranges 0.1 to 20 mm, and for >20 mm we have a decrease of MAE for MKF schemes from d02 to d03, from 16 mm to about 12.5 mm. Simulations KF_MIL and MKF_MIL seem to have a perfect score for BIAS in d03 (not shown).

The RMSE, between the forecast and observed values, along with the ratio of the two standard deviations of the two patterns, are all indicated by a single point on a two dimensional plot (see Fig. 9) proposed by Taylor (2001). The aim of such polar style graphs, which use the geometric relationship between the correlation (R), RMSE, σ_f and σ_o, is to quantify how close the forecast values of the different simulations are compared to observations. They are also very useful to monitor how accurately a model simulates the accumulated rainfall. On the plots, number 1 refers to the reference value, the rain gauge observations, while the numbers from 2 to 10 represent the 9 simulations that we performed at both d02 (Fig. 9a, c and e) and d03 (Fig. 9b, d and f).

Fig. 9a shows that all simulations at the period 00:00–06:00 UTC, in d02 underestimate the amplitude of the precipitation and they are not well correlated with the observations. The best simulation seems to be MKF_MOR (#9) which is closest to the reference curve, with $R = 0.77$ and the worst simulation is the MKF_NTH (#10), even though MKF_MIL (#8) has worse R, it has a slightly longer distance from the reference curve with the largest σ_f. In Fig. 9b we can clearly see better performance of all d03 simulations, compared to d02, but again all the simulations underestimate the observed precipitation. The MKF_MOR (#9) simulation of d03 has again the best performance among the others with R ~ 0.8 and the lowest RMSE. The worst simulations are those that use the GRF CPS.

Fig. 9c shows that all simulations at the period 06:00–12:00 UTC, in d02 underestimate the precipitation amounts, but MKF_MIL (#8) and MKF_MOR (#9) have the lowest distance from the reference curve. Even though the models with Kain-Fritsch CPS (#6–7) have better R and RMSE, MKF_MOR (#9) is the best simulation during this period, with the lowest σ_f. Fig. 9d refers to the d03 simulations and it is worth noticing that two simulations slightly overestimate the precipitation amount. MKF_MIL (#8) seems to be the best simulation, even though its R is lower than MKF_MOR (#9), as it has lower σ_f. The worst simulations are those that use the Morrison scheme with GRF and KF CPSs.

In the overall model performance period (00:00–12:00 UTC), summarized in Fig. 9e–f, MKF_MOR (#9) shows the best skill, with the lowest σ_f and the second lowest RMSE. Moreover, it is clear that d03 forecast skill is improved compared to d02, and the improvement is larger for simulations GRF_MIL (#2), KF_MIL (#5) and MKF_NTH (#10).

3.4. Analysis of the MCS

Based on the results of the verification procedure, we conclude that the MKF_MOR simulation is the best among the other eight simulations, with the best overall scores. For that reason, for the subsequent analysis of the MCS, the model output from this simulation is used. Fig. 10a shows the equivalent potential temperature (θ_e) at 850 hPa and therefore the position of the cold front, with the unstable air masses just in front of it. Also, Fig. 10b presents the low level convergence line in accordance with model reflectivity (Fig. 10c) and the exact position of the linear convective system at 03:00 UTC, which is verified by the observations in Section 2. Moreover, Fig. 10d depicts the mixed layer CAPE values and the deep layer wind shear (0–6 km) with values at 03:00 UTC that are verified by the Nimes-Courbessac sounding (Fig. 2a). Highly unstable air masses with 850 hPa θ_e values near 60 °C and 1000–2000 J kg^{-1} mixed layer CAPE (for parcels with mean layer values of temperature and moisture from the lowest 100 hPa) were found over a low level horizontal convergence zone with values near 10^{-4} s^{-1}. The strong DLS, which was also directional, was ancillary in organizing the MCS in a linear form, assisted by a mid level (500 hPa) flow of 26 m s^{-1}.

For the interpolation of rainfall observations on a regular grid an inverse distance weighted interpolation algorithm was used over a grid consisting of 400 × 300 grid points, fairly close to d03 horizontal grid increment. In Fig. 11a, the considered simulation (MKF_MOR) underestimates the precipitation peak observed over CV, and there are also strong differences in pattern and position between observations and forecast. A rather good agreement between observed and forecast rain accumulation for the period 00:00–06:00 UTC is evident, except from the light rain (0.5–5 mm) which was forecast over the Var department but it was not verified. For the second 6-hour period, in Fig. 12, the model underestimated the rainfall in CV, Ardèche and Var departments as it failed to simulate the MCS that moved near the coasts of Gulf of Genoa and produced heavy rain of >30 mm in 3 h. On the contrary, it succeeded in simulating the stratiform rain behind the cold front. To sum up, in Fig. 13, the MKF_MOR simulation, but also all the other simulations that were performed (not shown), underestimated the 12-hour accumulated precipitation but also the amplitude of maximum rainfall in CV region.

3.5. Microphysical analysis of the storm

Ribaud et al. (2016) performed an evaluation of a fuzzy logic hydrometeor classification algorithm (HCA), which can discriminate six microphysical species regardless the radar wavelength, by using multi-frequency polarimetric radar data collected during the SOP1 campaign. One of the case studies analyzed by the authors was the bow echo system of 24 September 2012. The authors managed to provide a detailed view of the microphysical structure of this MCS between 23:30 UTC on 23 September and 03:30 UTC on 24 September 2012. This provides an excellent opportunity to also evaluate the WRF performance in representing the 3D distribution of the microphysical species.

The WRF model output at 02:00 UTC was used, approximately corresponding to the period between 01:30 UTC and 01:45 UTC when the maximum intensity of the bow-echo system was observed (Ribaud et al., 2016, Figs. 2a, 7). Fig. 14a shows the model derived reflectivity at 3 km above mean sea level height (AMSL) at 02:00 UTC, while the black box represents the domain that Ribaud et al. (2016) used for their study. The model was able to place the convective system at the correct position, with a spatial displacement of only a few kilometers, and to reproduce successfully the orientation of the convective line axis. Fig. 14b shows a vertical cross section of the simulated reflectivity

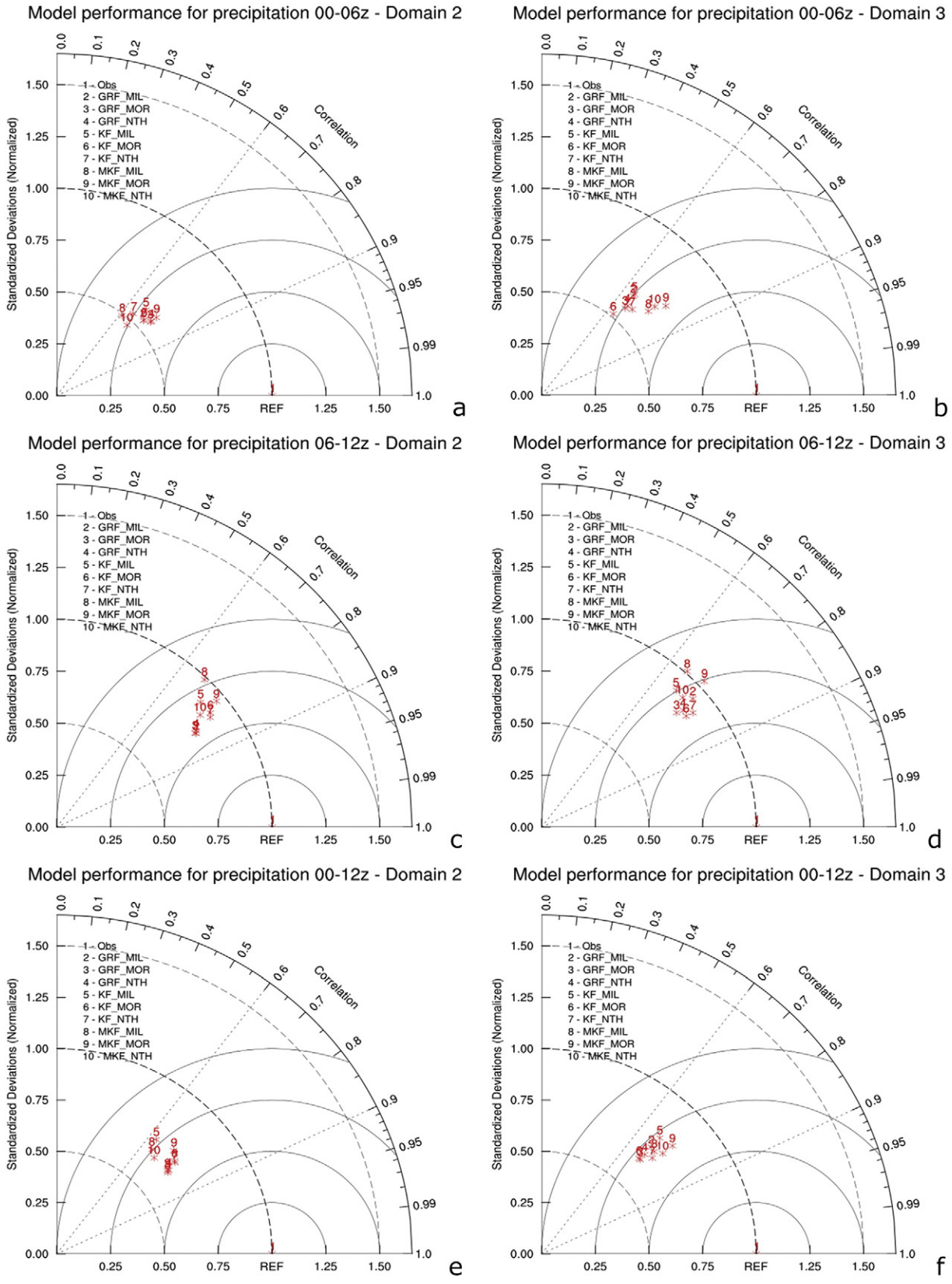

Fig. 9. Normalized pattern statistics showing differences between the observational rainfall and the nine model simulations over the two higher domains d02 (a, c and e) and d03 (b, d and f) and for the three considered time periods: 00–06z (a–b); 06–12z (c–d); and 00–12z (e–f).

at 02:00 UTC along the black horizontal line within the black box of Fig. 14a. Fig. 14c shows a vertical cross section of the simulated graupel and ice mixing ratios along the same line.

Comparison of the model derived reflectivity with the observed one by the radars shows a good agreement (not shown). Ribaud et al. (2016) found reflectivity values exceeding 50 dBz at ~2 km and an

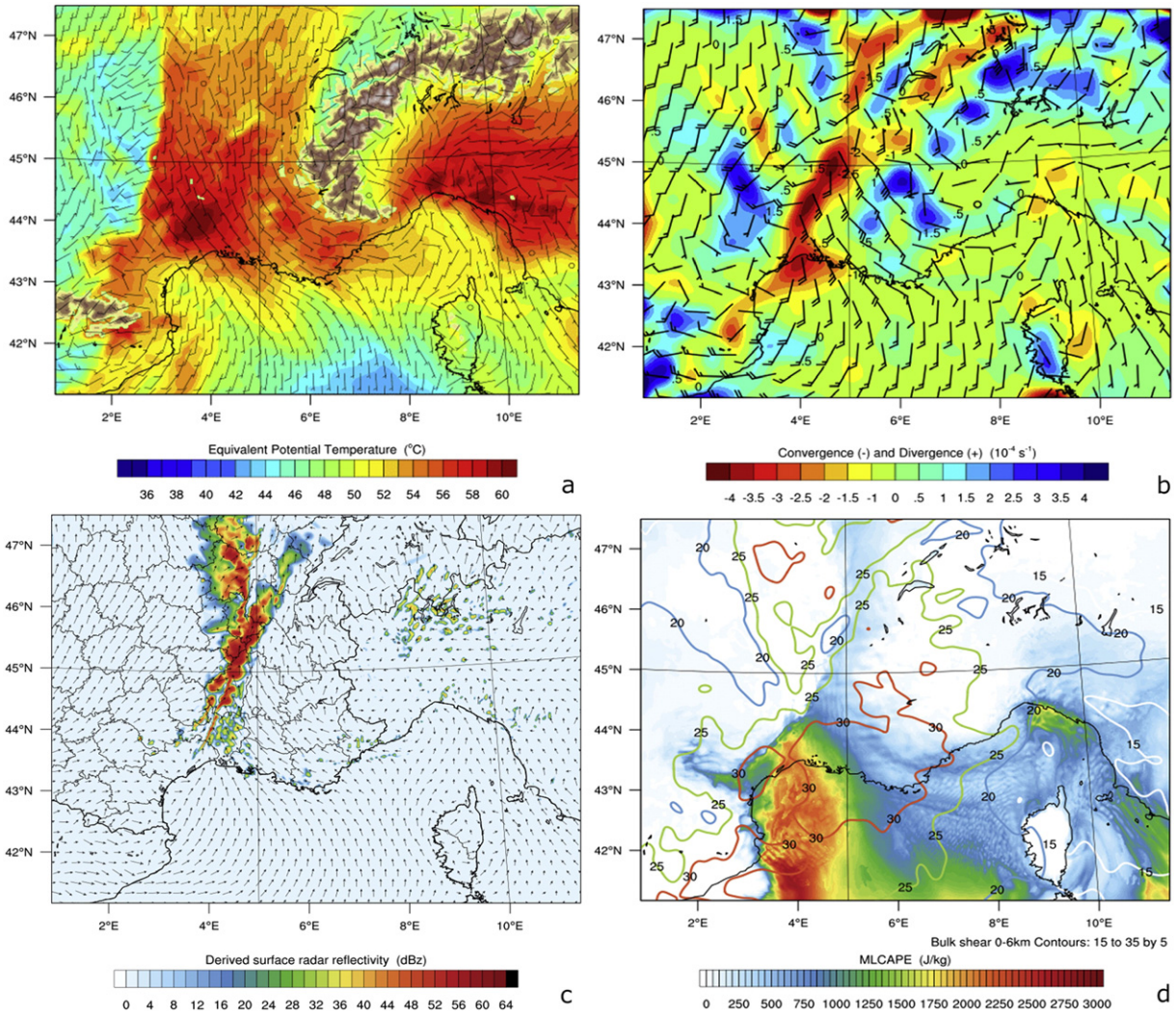

Fig. 10. MKF_MOR simulation for d03 at 03:00 UTC on 24 September 2012: (a) Equivalent potential temperature at 850 hPa and 10-m wind (in barbs), (b) low level convergence (0–200 m) and 10-m wind, (c) model derived reflectivity (dBz) and (d) mixed layer CAPE in J kg^{-1} (shaded) with DLS (contours).

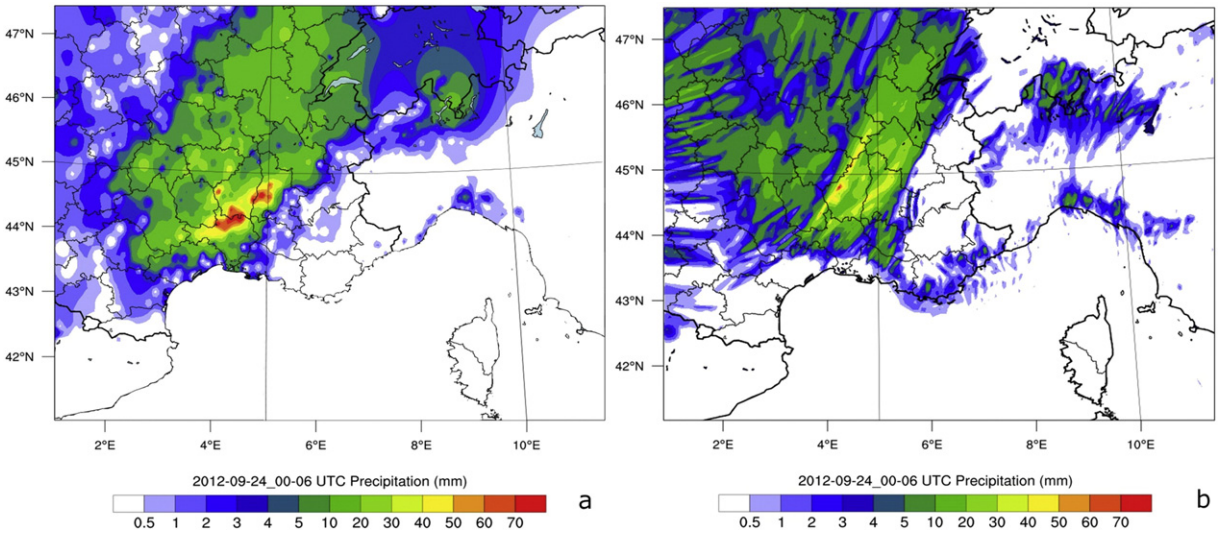

Fig. 11. (a) 6-h accumulated total precipitation from rain gauges and (b) total precipitation from MKF_MOR simulation during the period 00:00–06:00 UTC 24 September 2012.

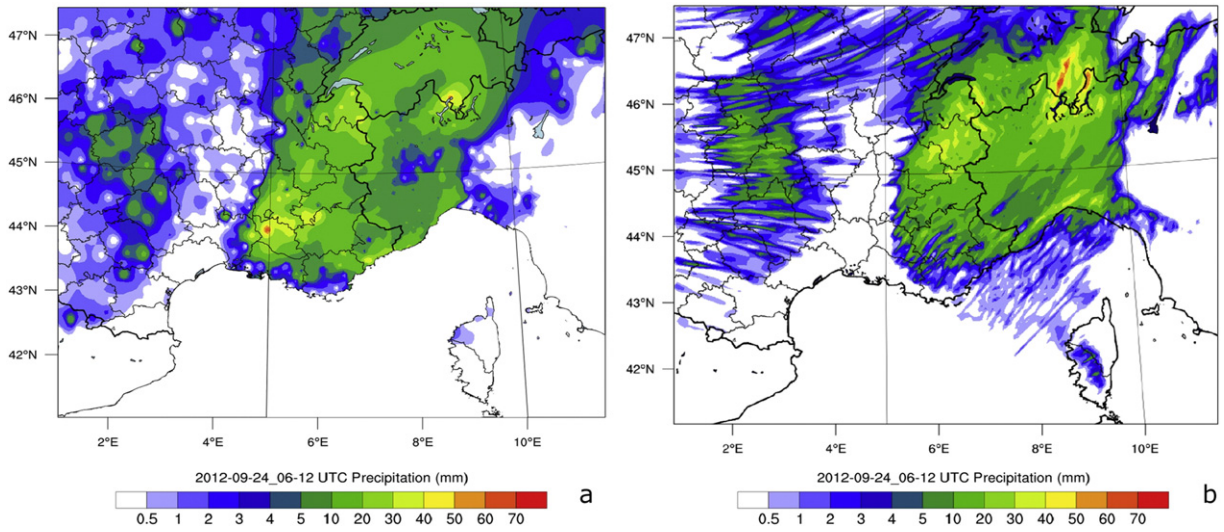

Fig. 12. (a) 6-h accumulated total precipitation from rain gauges and (b) total precipitation from MKF_MOR simulation during the period 06:00–12:00 UTC 24 September 2012.

extent of the 25 dBz isoline up to ~11 km (see their Fig. 7c). The simulated reflectivity shows a correctly positioned maximum within the layer 2–3 km exceeding 50 dBz, while above 3 km AMSL the model values are slightly underestimated compared to the observed ones. The simulated cell reaches almost 11 km (as inferred by the 25 dBz isoline) which again agrees with the observed height. Ribaud et al. (2016) found the presence of a hail column that extends from the surface up to a height of 4 km and the HCA shows that the graupel exists from 3 to 10 km AMSL. Since the Morrison microphysical scheme used for this simulation (MKF_MOR) cannot explicitly calculate the hail formation, it is possible to infer the presence of hail from the simulated reflectivity (Fig. 14b) assuming that when values exceed 55 dBz this might indicate the presence of hail near the surface (Skripniková and Řezáčová, 2014). Hail occurrence was verified by observers at 02:00 UTC (Ribaud et al., 2015). The MKF_MOR simulation produces graupel from just above the freezing level height (3.5 km) up to 10 km, in agreement with the HCA output, although the model underestimates the mixing ratio of ice with only a limited coverage above 8 km AMSL (Fig. 14c). At 02:00 UTC the maximum vertical velocity estimated by the ground radars was 12 m s^{-1} (see Fig. 14d) while the cloud tops were found at an altitude of 10 km, creating a wide anvil (Ribaud et al., 2016, see their Fig. 8c). The MKF_MOR simulation slightly overestimated the maximum vertical velocity (14.2 m s^{-1}) while the model-derived reflectivity was up to 45 dBz at 6 km AMSL, in accordance with radar measurements. A final investigation of the microphysical structure of the MCS, inside the box area shown in Fig. 14a, was performed by averaging the mixing ratio of graupel derived from the model simulation MKF_MOR. Values between 5 and 8 km AMSL for graupel were compared against the evolution of lightning activity from 00:00 up to 09:00 UTC (Fig. 15a). This tropospheric layer was selected as it was found that the concentration of graupel was the highest within it. Fig. 15b shows the maximum vertical velocity w (m s^{-1}) during the same period, indicating strong updrafts within this area, for 00:00 UTC up to 07:00 UTC and then a sharp decrease up to 09:00 UTC. Comparison of graupel and vertical velocity temporal evolution against the lightning activity underlines the role of graupel concentrations on the electrification processes, as the sharp decrease of lightning activity evident between 03:00–04:00 UTC is associated with reduced graupel concentrations, while again the next peak of lightning at 07:00 UTC is clearly associated with a sharp increase of graupel concentrations.

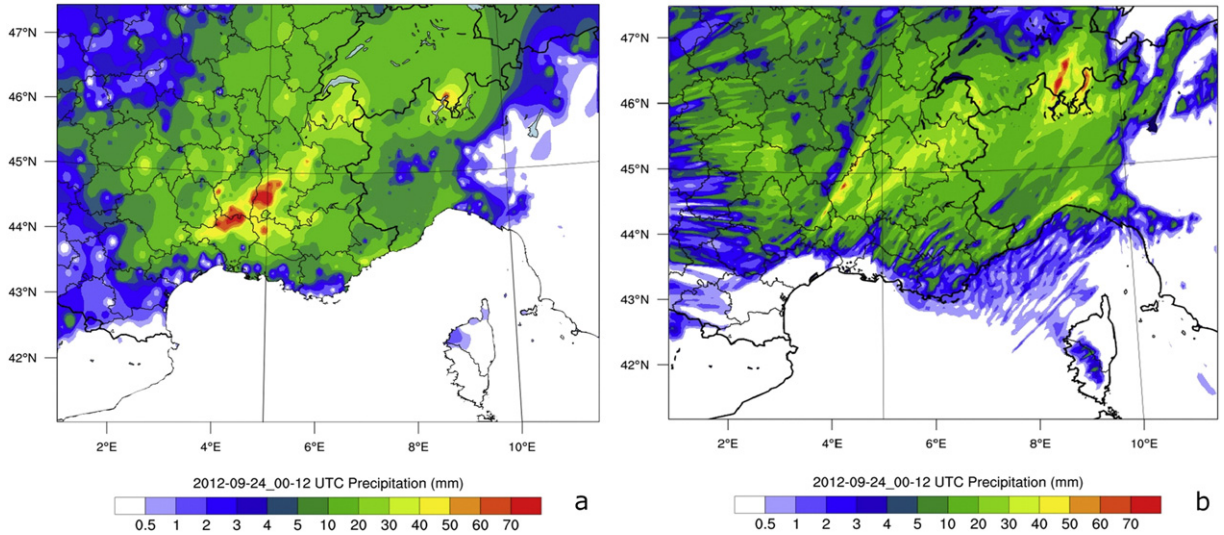

Fig. 13. (a) 12-h accumulated total precipitation from rain gauges and (b) total precipitation from MKF_MOR simulation during the period 00:00–12:00 UTC 24 September 2012.

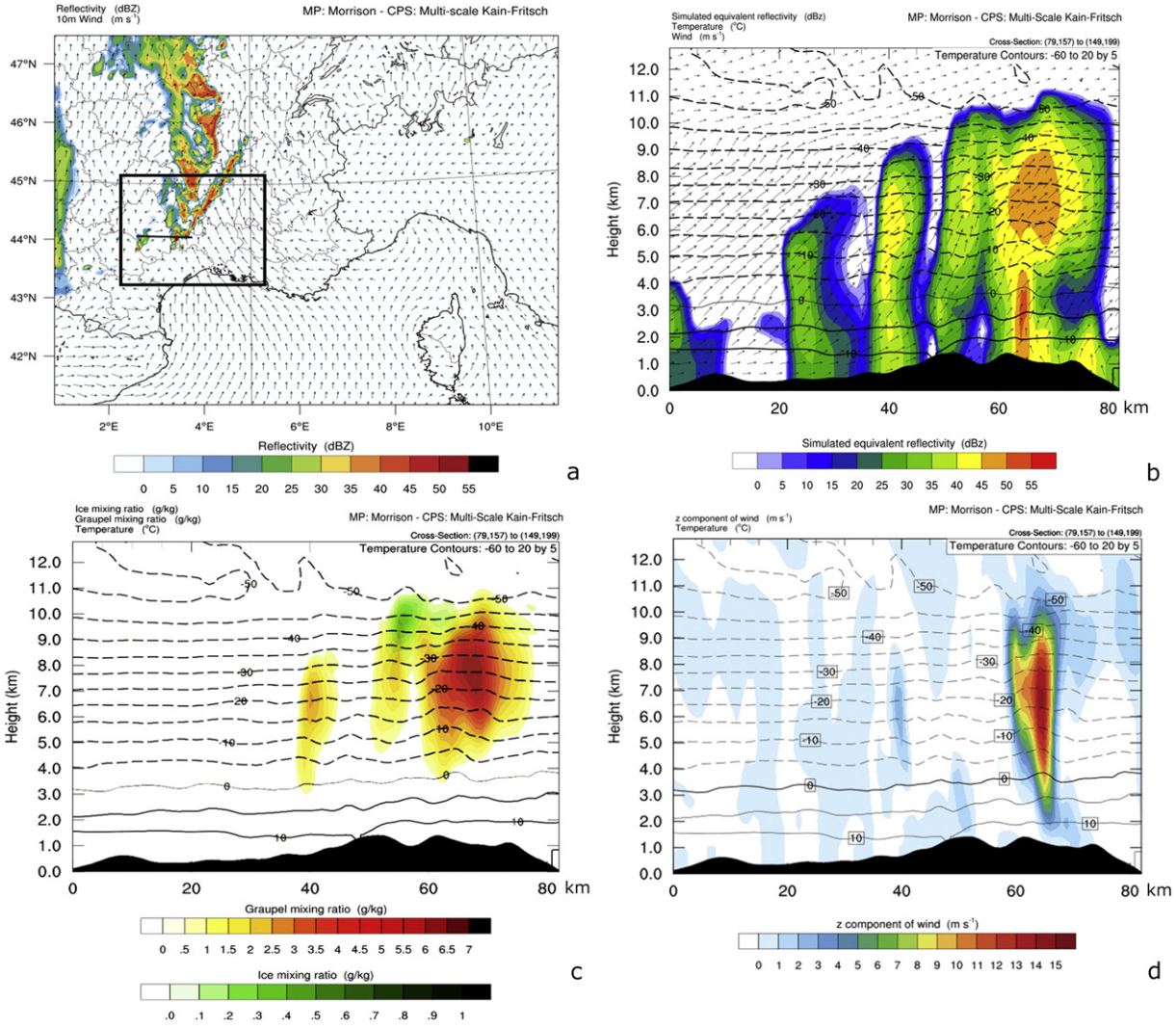

Fig. 14. (a) Model derived reflectivity at 3 km above mean sea level height and 10-m wind speed at 02:00 UTC on 24 September 2012, (b) a vertical cross section of simulated equivalent reflectivity (dBz) (shaded), temperature isotherms (°C) and wind speed (arrows) at 02:00 UTC, (c) a vertical cross section of graupel mixing ratio (g kg^{-1}) and (d) a vertical cross section of ice mixing ratio (g kg^{-1}) at 02:00 UTC.

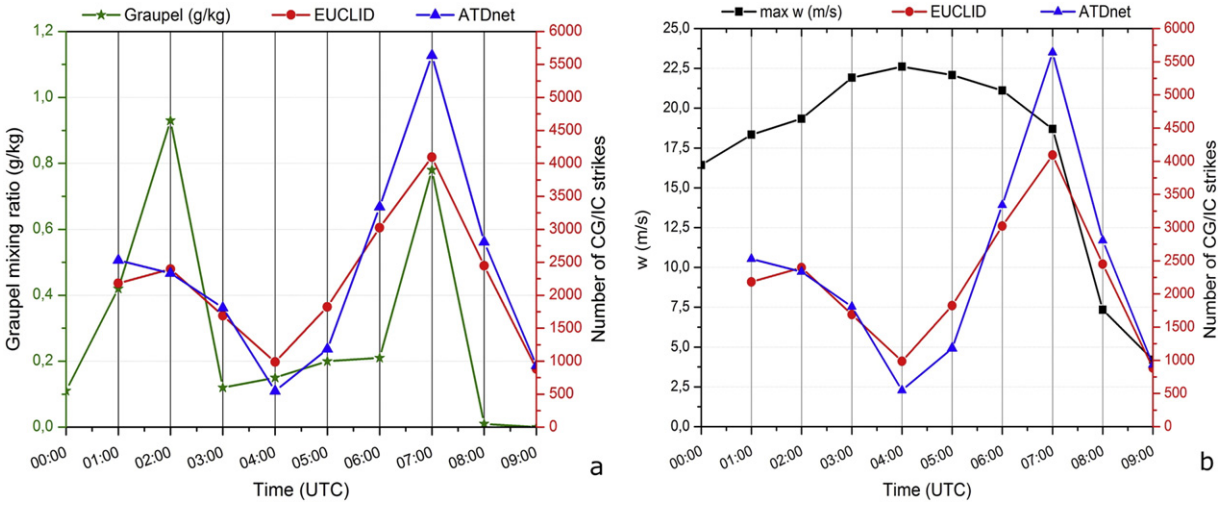

Fig. 15. (a) Time series of model derived average graupel mixing ratio (g kg^{-1}) and lightning strike resources from ATDnet and EUCLID networks, (b) maximum vertical velocity (m s^{-1}) between 00:00 and 09:00 UTC for the domain described in Fig. 14a.

4. Summary and conclusions

An intense fast moving linear convective system, associated with excessive rain and exceptionally high lightning activity (Ribaud et al., 2016), affected the southern parts of France and especially the southern Massif Central foothills the early morning of 24 September 2012, during the HyMeX — SOP1 campaign. The MCS had the structure of a bow echo system with a V-shape feature visible in the infrared satellite imagery and a linear convective signature on the radar echoes. Mesoscale processes (vorticity advection, upper-level PV anomalies, strong low-level moisture advection, CAPE, etc.) and local convergence zones created a favorable environment for deep moist convection development. Numerous rain gauges recorded high values of accumulated convective precipitation, in fact the highest values during the 3-month SOP1 campaign.

In the frame of this work model simulations using WRF non-hydrostatic model with activation of various microphysical and convective parameterization schemes are evaluated. The high-resolution simulations reproduce fairly well the significant rainfall amounts associated with the MCS, but all of them underestimate the accumulated precipitation.

The numerical experiment that best reproduces the event is used to identify the physical mechanisms leading to this convective episode. A study of the life cycle of the microphysical distribution is carried out based on model output. The results are intercompared with recent literature, namely with the work of Ribaud et al. (2016) where a sophisticated algorithm of hydrometeors (HCA) is used. The results show that the model is able to correctly place the MCS and the three dimensional distribution of hydrometeors, and it is in an overall agreement with the HCA, reproducing an environment that can support the production of intense lightning activity. Moreover, WRF simulations are able to show that during the phase of reduced lighting activity (03:00 to 05:00 UTC) the graupel concentrations within the layer 5–8 km show a clear minimum, affecting thus the electrification processes, although in the same time frame vertical velocities (both reproduced by WRF model and estimated by radar measurements, as shown in Ribaud et al., 2016) are exceptionally high.

The work presented here shows the need to use high-resolution modeling and sophisticated microphysical schemes in order to better reproduce the MCS structures. It is also shown that model validation is highly dependent on the availability of detailed measurements, as the ones gathered during HyMeX — SOP1. It is in the authors' interests to extend this kind of investigation to systems affecting the eastern Mediterranean area and therefore the need of an experimental campaign in the East, as already mentioned in the HyMeX scientific plan, is considered necessary.

Acknowledgements

The authors acknowledge Météo-France for supplying the Nimes' radar data and Nimes-Courbessac radiosonde measurements. The authors also acknowledge Météo-France and the HyMeX program for supplying the rain gauge data, sponsored by Grants MISTRALS/HyMeX and ANR-11-BS56-0005 IODA-MED project. Moreover, we are grateful to EUMETSAT and LATMOS for supplying the MSG RSS data and the HyMeX database teams (ESPRI/IPSL and SEDOO/OMP) for their help in accessing the data collected for the SOP1 case studies.

References

Anderson, G., Klugmann, D., 2014. A European lightning density analysis using 5 years of ATDnet data. Nat. Hazards Earth Syst. Sci. 14, 815–829.

Arakawa, A., 2004. The cumulus parameterization problem: past, present, and future. J. Clim. 17, 2493–2525.

Bennett, A.J., Odams, P., Edwards, D., Arason, Þ., 2010. Monitoring of lightning from the April–May 2010 Eyjafjallajökull volcanic eruption using a very low frequency lightning location network. Environ. Res. Lett. 5:044013. http://dx.doi.org/10.1088/1748-9326/5/4/044013 (October–December 2010).

Bousquet, O., et al., 2015. Multifrequency radar observations collected in southern France during HyMeX-SOP1. Bull. Am. Meteorol. Soc. 96 (2), 267–282.

Browning, K.A., Golding, B.W., 1995. Mesoscale aspects of a dry intrusion within a vigorous cyclone. Q. J. R. Meteorol. Soc. 121, 463–493.

Cecil, D.J., Buechler, D., Blakeslee, R.J., 2014. Gridded lightning climatology from TRMM-LIS and OTD: dataset description. Atmos. Res. 136, 404–414.

Defer, E., Pinty, J.-P., Coquillat, S., Martin, J.-M., Prieur, S., Soula, S., Richard, E., Rison, W., Krehbiel, P., Thomas, R., Rodeheffer, D., Vergeiner, C., Malaterre, F., Pedeboy, S., Schulz, W., Farges, T., Gallin, L.-J., Ortéga, P., Ribaud, J.-F., Anderson, G., Betz, H.-D., Meneux, B., Kotroni, V., Lagouvardos, K., Roos, S., Ducrocq, V., Roussot, O., Labatut, L., Molinié, G., 2015. An overview of the lightning and atmospheric electricity observations collected in Southern France during the HYdrological cycle in Mediterranean EXperiment (HyMeX), Special Observation Period 1. Atmos. Meas. Tech. 8, 649–669.

Delrieu, G., et al., 2005. The catastrophic flash-flood event of 8–9 September 2002 in the Gard region, France: a first case-study for the Mediterranean Hydrometeorological Observatory. J. Hydrometeorol. 6, 34–52.

Dotzek, N., Groenemeijer, P., Feuerstein, B., Holzer, A.M., 2009. Overview of ESSL's severe convective storms research using the European Severe Weather Database ESWD. Atmos. Res. 93, 575–586.

Drobinski, P., Ducrocq, V., Alpert, P., Anagnostou, E., Béranger, K., Borga, M., Braud, I., Chanzy, A., Davolio, S., Delrieu, G., Estournel, C., Filali Boubrahmi, N., Font, J., Grubisic, V., Gualdi, S., Homar, V., Ivancan-Picek, B., Kottmeier, C., Kotroni, V., Lagouvardos, K., Lionello, P., Llasat, M.C., Ludwig, W., Lutoff, C., Mariotti, A., Richard, E., Romero, R., Rotunno, R., Roussot, O., Ruin, I., Somot, S., Taupier-Letage, I., Tintore, J., Uijlenhoet, R., Wernli, H., 2014. HyMeX: a 10-year multidisciplinary program on the Mediterranean water cycle. Bull. Am. Meteorol. Soc. 95, 1063–1082.

Ducrocq, V., Aullo, G., Santurette, P., 2003. Les precipitations intenses et les inondations du 12 et 13 Novembre 1999 sur le sud de la France. La Meteorologie 8th serie 42 pp. 18–27.

Ducrocq, V., et al., 2004. L'evenement des 8–9 Septembre 2002: situation meteorologique et simulation a mesoechelle. La Houille Blanche 6, 86–92.

Ducrocq, V., Nuissier, O., Ricard, D., Lebeaupin, C., Thouvenin, T., 2008. A numerical study of three catastrophic precipitating events over western Mediterranean region (southern France). Part II: mesoscale triggering and stationarity factors. Q. J. R. Meteorol. Soc. 134, 131–145.

Ducrocq, V., Braud, I., Davolio, S., Ferretti, R., Flamant, C., Jansa, A., Kalthoff, N., Richard, E., Taupier-Letage, I., Ayral, P.-A., Belamari, S., Berne, A., Borga, M., Boudevillain, B., Bock, O., Boichard, J.-L., Bouin, M.-N., Bousquet, O., Bouvier, C., Chiggiato, J., Cimini, D., Corsmeier, U., Coppola, L., Cocquerez, P., Defer, E., Delanoë, J., Di Girolamo, P., Doerenbecher, A., Drobinski, P., Dufournet, Y., Fourrié, N., Gourley, J.J., Labatut, L., Lambert, D., Le Coz, J., Marzano, F.S., Molinié, G., Montani, A., Nord, G., Nuret, M., Ramage, K., Rison, W., Roussot, O., Said, F., Schwarzenboeck, A., Testor, P., Van Baelen, J., Vincendon, B., Aran, M., Tamayo, J., 2014. HyMeX-SOP1: the field campaign dedicated to heavy precipitation and flash flooding in the northwestern Mediterranean. Bull. Am. Meteorol. Soc. 95, 1083–1100.

Dudhia, J., 1989. Numerical study of convection observed during the Winter Monsoon Experiment using a mesoscale two-dimensional model. J. Atmos. Sci. 46, 3077–3107.

Federico, S., Avolio, E., Bellecci, C., Colacino, M., Lavagnini, A., Accadia, C., Mariani, S., Casaioli, M., 2004. Three model intercomparison for quantitative precipitation forecast over Calabria. Il Nuovo Cimento C 27, 627–647.

Flaounas, E., Raveh-Rubin, S., Wernli, H., Drobinski, P., Bastin, S., 2015. The dynamical structure of intense Mediterranean cyclones. Clim. Dyn. 44:2411. http://dx.doi.org/10.1007/s00382-014-2330-2.

Flaounas, E., Lagouvardos, K., Kotroni, V., Claud, C., Delanoë, J., Flamant, C., Madonna, E., Wernli, H., 2016. Processes leading to heavy precipitation associated with two Mediterranean cyclones observed during the HyMeX SOP1. Q. J. R. Meteorol. Soc. 142: 275–286. http://dx.doi.org/10.1002/qj.2618.

Fritsch, J.M., et al., 1998. Quantitative precipitation forecasting: report of the eighth prospectus development team, U.S. Weather Research Program. Bull. Am. Meteorol. Soc. 79, 285–299.

Gao, S.T., Cao, J., 2007. Physical basis of generalized potential temperature and its application to cyclone tracks in non-uniformly saturated atmosphere. J. Geophys. Res. 112 (D18101), 1–7.

Godart, A., Leblois, E., Anquentin, S., Freychet, N., 2010. Analysis of the relationship between banded orographic convection and atmospheric properties using factorial discriminant analysis and neural networks. J. Appl. Meteorol. Climatol. 49:646–663. http://dx.doi.org/10.1175/2009JAMC2217.1.

Hally, A., Richard, E., Ducrocq, V., 2014. An ensemble study of HyMeX IOP6 and IOP7a: sensitivity to physical and initial and boundary condition uncertainties. Nat. Hazards Earth Syst. Sci. 14 (1071–1084):2014. http://dx.doi.org/10.5194/nhess-14-1071-2014.

Hong, S.Y., Yign, N., Dudhia, J., 2006. A new vertical diffusion package with an explicit treatment of entrainment processes. Mon. Weather Rev. 134, 2318–2341.

Houze Jr., R.A., 2004. Mesoscale convective systems. Rev. Geophys. 42, RG4003. http://dx.doi.org/10.1029/2004RG000150.

Huet, P., Martin, X., Prime, J.L., Foin, P., Laurain, C., Cannard, P., 2003. Retour d'expériences des crues de septembre 2002 dans les départements du Gard, de l'Hérault, du Vaucluse, des bouches du Rhône, de l'Ardèche et de la Drôme. Inspection générale de l'Environnement, Paris, France (124 pp).

Jansa, A., Alpert, P., Arbogast, P., Buzzi, A., Ivancan-Picek, B., Kotroni, V., Llasat, M.C., Ramis, C., Richard, E., Romero, R., Speranza, A., 2014. MEDEX: a general overview. Nat. Hazards Earth Syst. Sci. 14, 1965–1984.

Kain, J.S., 2004. The Kain–Fritsch convective parameterization: an update. J. Appl. Meteorol. 43:170–181. http://dx.doi.org/10.1175/1520-0450.

Kotroni, V., Lagouvardos, K., 2001. Precipitation forecast skill of different convective parameterization and microphysical schemes: application for the cold season over Greece. Geophys. Res. Lett. 28 (10), 1977–1980.

Kotroni, V., Lagouvardos, K., 2008. Lightning occurrence in relation with elevation, terrain slope and vegetation cover in the Mediterranean. J. Geophys. Res. 113, D21118. http://dx.doi.org/10.1029/2008JD010605.

Lagouvardos, K., Kotroni, V., 2000. Use of METEOSAT water-vapour images for the diagnosis of a vigorous stratospheric intrusion over the central Mediterranean. Meteorol. Appl. 7:205–210. http://dx.doi.org/10.1017/S1350482700001596.

Lagouvardos, K., Kotroni, V., Koussis, A., Feidas, C., Buzzi, A., Malguzzi, P., 2003. The meteorological model BOLAM at the National Observatory of Athens: assessment of two-year operational use. J. Appl. Meteorol. 42, 1667–1678.

Lagouvardos, K., Kotroni, V., Betz, H.-D., Schmidt, K., 2009. A comparison of lightning data provided by ZEUS and LINET networks over Western Europe. Nat. Hazards Earth Syst. Sci. 9, 1713–1717.

Lagouvardos, K., Kotroni, V., Defer, E., Bousquet, O., 2013. Study of a heavy precipitation event over southern France, in the frame of HYMEX project: observational analysis and model results using assimilation of lightning. Atmos. Res. 134, 45–55.

Lefrou, C., Martin, X., Labarthe, J.-P., Varret, J., Mazière, B., Tordjman, R., Feunteun, R., 2000. Les crues des 11, 12 et 13 novembre 1999, dans les départements de l'Aude, l'Hérault, les Pyrennées Orientales et du Tarn. Inspection générale de l'Environnement, Paris, France (140 pp.).

Llasat, M.C., Llasat-Botija, M., Petrucci, O., Pasqua, A.A., Rosselló, J., Vinet, F., Boissier, L., 2013. Towards a database on societal impact of Mediterranean floods within the framework of the HyMeX project. Nat. Hazards Earth Syst. Sci. 13:1337–1350. http://dx.doi.org/10.5194/nhess-13-1337-2013.

Lund, N.R., MacGorman, D.R., Schuur, T.J., Biggerstaff, M.I., Rust, W.D., 2009. Relationships between lightning location and polarimetric radar signatures in a small mesoscale convective system. Mon. Weather Rev. 137, 4151–4170.

Markowski, P., Richardson, Y., 2010. References, in Mesoscale Meteorology in Midlatitudes. John Wiley & Sons, Ltd, Chichester, UK http://dx.doi.org/10.1002/9780470682104.refs.

Mazarakis, N., Kotroni, V., Lagouvardos, K., Argiriou, A.A., 2009. The sensitivity of numerical forecasts to convective parameterization during the warm period and the use of lighting data as an indicator for convective occurrence. Atmos. Res. 94, 704–714.

Milbrandt, J.A., Yau, M.K., 2005. A multimoment bulk microphysics parameterization. Part I: analysis of the role of the spectral shape parameter. J. Atmos. Sci. 62, 3051–3064.

Mlawer, E.J., Taubman, S.J., Brown, P.D., Iacono, M.J., Clough, S.A., 1997. Radiative transfer for inhomogeneous atmospheres: RRTM, a validated correlated-k model for the longwave. J. Geophys. Res. 102, 16663–16682.

Morrison, H., Thompson, G., Tatarskii, V., 2009. Impact of cloud microphysics on the development of trailing stratiform precipitation in a simulated squall line: comparison of one- and two-moment schemes. Mon. Weather Rev. 137, 991–1007.

Newman, J.F., Heinselman, P.L., 2012. Evolution of a quasi-linear convective system sampled by phased array radar. Mon. Weather Rev. 140:3467–3486. http://dx.doi.org/10.1175/MWR-D-12-00003.1.

Nuissier, O., et al., 2008. A numerical study of three catastrophic precipitating events over southern France. I: numerical framework and synoptic ingredients. Q. J. R. Meteorol. Soc. 134:111–130. http://dx.doi.org/10.1002/qj.200.

Papagiannaki, K., Lagouvardos, K., Kotroni, V., 2013. A database of high-impact weather events in Greece: a descriptive impact analysis for the period 2001–2011. Nat. Hazards Earth Syst. Sci. 13, 727–736.

Parker, M.D., Johnson, R.H., 2000. Organizational modes of midlatitude-mesoscale convective systems. Mon. Weather Rev. 128, 3413–3436.

Poelman, D.R., Schulz, W., Vergeiner, C., 2012. Performance characteristics of three distinct lightning detection networks covering Belgium. 22nd International Lightning Detection Conference, 2–3 April, Colorado, USA.

Ribaud, J.-F., Bousquet, O., Coquillat, S., Al-Sakka, H., Lambert, D., Ducrocq, V., Fontaine, E., 2015. Evaluation and application of hydrometeor classification algorithm outputs inferred from multi-frequency dual-polarimetric radar observations collected during HyMeX. Q. J. R. Meteorol. Soc. 142, 95–107.

Ribaud, J.-F., Bousquet, O., Coquillat, S., 2016. Relationships between total lightning activity, microphysics, and kinematics during the 24 September 2012 HyMeX bow echo system. Q. J. R. Meteorol. Soc. 142:298–309. http://dx.doi.org/10.1002/qj.2756.

Ricard, D., Ducrocq, V., Auger, L., 2012. A climatology of mesoscale environment associated with Mediterranean Heavy Precipitating Events over a Northwestern Mediterranean area. J. Appl. Meteorol. Climatol. 51, 468–488.

Senesi, S.P., et al., 1996. The Vaison-la-Romaine flash flood: mesoscale analysis and predictability issues. Weather Forecast. 11, 417–442.

Shuai, Y., Xiaopeng, C., Lingkum, R., 2009. Analyses of dry intrusion and instability during a heavy rainfall event that occurred in northern China. Atmos. Ocean Sci. Lett. 2 (2), 108–112.

Skamarock, W.C., et al., 2008. A description of the advanced research WRF version 3. NCAR Tech. Note NCAR/TN-475 + STR (113 pp).

Skripniková, K., Řezáčová, D., 2014. Radar-based hail detection. Atmos. Res. 144:175–185. http://dx.doi.org/10.1016/j.atmosres.2013.06.002.

Taylor, K.E., 2001. Summarizing multiple aspects of model performance in a single diagram. J. Geophys. Res. 106 (D7):7183–7192. http://dx.doi.org/10.1029/2000JD900719/abstract.

Tewari, M., Chen, F., Wang, W., Dudhia, J., LeMone, M., Mitchell, K., Ek, M., Gayno, G., Weigel, J., Cuenca, R., 2004. Implementation and Verification of the Unified Noah Land Surface Model in the WRF Model, Paper Presented at the20th Conference on Weather Analysis and Forecasting/16th Conference on Numerical Weather Prediction. Am. Meteorol. Soc., Seattle, Wash. (Jan 11–15 2004).

Thompson, G., Field, P.R., Rasmussen, R.M., Hall, W.D., 2008. Explicit forecasts of winter precipitation using an improved bulk microphysics scheme. Part II: implementation of a new snow parameterization. Mon. Weather Rev. 136, 5095–5115.

Wiens, K.C., Rutledge, S.A., Tessendorf, S.A., 2005. The 29 June 2000 supercell observed during STEPS. Part II: lightning and charge structure. J. Atmos. Sci. 62, 4151–4177.

Yair, Y., Shalev, S., Erlich, Z., Agrachov, A., Katz, E., Saaroni, H., Price, C., Ziv, B., 2014. Lightning flash multiplicity in eastern Mediterranean thunderstorms. Nat. Hazards Earth Syst. Sci. 14, 165–173.

Zheng, Y., Alpaty, K., Herwehe, J.A., Del Genio, A.D., Niyogi, D., 2016. Improving high-resolution weather forecasts using the Weather Research and Forecasting (WRF) model with an updated Kain-Fritsch scheme. Mon. Weather Rev. 144 (3):833–860. http://dx.doi.org/10.1175/MWR-D-15-0005.1.